Integrated Study of Existing Tsunami Design Standards

Nicolette S. Lewis[1]; Dawn E. Lehman, A.M.ASCE[2]; Michael R. Motley, A.M.ASCE[3]; Pedro Arduino, M.ASCE[4]; Charles W. Roeder, M.ASCE[5]; Christopher N. Pyke[6]; and Kenneth P. Sullivan[7]

Abstract: As the tsunami threat across the Pacific coast becomes better understood, vertical evacuation structures are being widely considered in order to improve life safety. The design of such structures requires careful consideration of fluid-induced forces. Recently, core walls have been used as a preferred system for lateral force resistance in tsunami-resistant structures. These structures require high strength and stiffness provided by walls both orthogonal and parallel to the demands; detailing and limiting shear stress demands provide the necessary ductility. There are, however, potential challenges to utilizing core wall systems for tsunami-resisting systems. Primarily, walls orthogonal to flow tend to draw large hydrodynamic and hydrostatic forces during tsunamis. Therefore, accurate estimates of these demands are needed for the design of resilient structures. A four-phase research program utilizing integrated experimental and numerical methods was undertaken to investigate these demands and the efficacy of current design standards in providing reasonable but conservative estimates for the forces imparted. The first phase of the program used computational fluid dynamics (CFD) to simulate the experiments, building on prior research. The second phase used the results from the simulations to define the bathymetry in the flume and the placement of instrumentation. In the third phase, a 1:6 prototypical scale core-wall structure was tested in the large wave flume at the Hinsdale Wave Research Laboratory, a Natural Hazards Engineering Research Infrastructure (NHERI) testing facility. The experimental setup permitted the testing of the full core-wall system, including the pile foundation and rough estimates of the impact of soil restraint on the demand. Strain gauges, load cells, and pressure distributions were used to provide advanced measurements of the structural response. These measurements were then used to validate the modeling approach. The fourth phase involved comparing the measured peak forces from experiments to standard design equations for imparted force against structures due to tsunami inundation using data acquired from the experiments with the intent of investigating tsunami load demand imparted to a structure after an earthquake. Earthquake loads were not taken into account in experimentation or analysis; they simply dictate a building's capacity against the initial event. **DOI: 10.1061/(ASCE)ST.1943-541X.0003506.**

Introduction

Along the Pacific coast, earthquakes and tsunamis are a significant risk, in particular in Hawaii and the Pacific northwest (PNW). Large magnitude subduction earthquakes may cause tsunamis, which could reach the coast within minutes after an earthquake. Based on geological evidence compiled by the US Geological Survey, every 525 years on average a major Cascadia subduction zone (CSZ) earthquake (i.e., with a moment magnitude of 9.0 or greater) that results in a tsunami can occur. Geological as well as Native American and Japanese historical records show that a significant seismic event occurred within the CSZ in the year 1700 (Atwater et al. 2015), generating a major tsunami that inundated the coasts of Washington, Oregon, and California, and an orphan tsunami that traveled across the Pacific Ocean to Japan (Petersen et al. 2014). The short travel time of tsunami waves generated in the ocean to nearby coastlines does not permit typical evacuation (i.e., travel away from the region or moving to higher ground) in low coastal regions. Numerous locations on the coasts of Washington, Oregon, California, and eastern Japan and western South America are susceptible to these events. As communities in the Pacific northwest of the United States have come to recognize the threat of the CSZ and its potential to produce both large magnitude earthquakes as well as incredibly destructive tsunamis, some have started to prepare for such events by constructing vertical evacuation structures. Vertical evacuation structures (VESs) may be the only practical method of protecting inhabitants located in low-lying coastal regions susceptible to tsunamis (Heintz and Mahoney 2008).

VESs are typically comprised of elevated shelters designed to resist forces from large-magnitude earthquakes and tsunamis; occupants of nearby buildings and communities can take refuge in these structures during a tsunami. To provide a safe refuge during sequential events, such structures must be designed to sustain inertial forces during earthquakes, fluid forces during tsunami inundation, and impact forces due to tsunami-borne debris. Consequently, engineers must design VESs with the strength and stiffness needed to support a large number of people above the inundation of a tsunami wave and to resist sequential earthquake and tsunami loads. ASCE 7-16 (ASCE 2017) provisions for tsunami loads and effects

[1]Ph.D. Student, Dept. of Civil & Environmental Engineering, Univ. of Washington, Seattle, WA 98004 (corresponding author). Email: nsaoirse@uw.edu

[2]Director of Large-Scale Structural Engineering Testing Laboratory, Dept. of Civil & Environmental Engineering, Univ. of Washington, Seattle, WA 98004. ORCID: https://orcid.org/0000-0002-0823-1167

[3]John R. Kiely Endowed Associate Professor in Civil & Environmental Engineering, Dept. of Civil & Environmental Engineering, Univ. of Washington, Seattle, WA 98004.

[4]H.R. Berg Endowed Professor in Civil & Environmental Engineering, Dept. of Civil & Environmental Engineering, Univ. of Washington, Seattle, WA 98004.

[5]Professor Emeritus of Civil & Environmental Engineering, Dept. of Civil & Environmental Engineering, Univ. of Washington, Seattle, WA 98004.

[6]Staff Engineer, Kleinschmidt Associates, 1500 NE Irving St., Suite 550, Portland, OR 97232. ORCID: https://orcid.org/0000-0003-4004-8597

[7]Engineer II, Bridge & Structural Unit, King County Department of Local Services, 201 South Jackson St., Seattle, WA 98104. ORCID: https://orcid.org/0000-0002-0055-5669

Note. This manuscript was submitted on October 4, 2021; approved on July 20, 2022; published online on October 7, 2022. Discussion period open until March 7, 2023; separate discussions must be submitted for individual papers. This paper is part of the ***Journal of Structural Engineering***, © ASCE, ISSN 0733-9445.

offer reasonable approximations for maximum building shear force magnitude in simplified conditions. The design equations are built from the fundamental physics of steady state flow in tsunami conditions and have proven to offer conservative values for the estimated base shear for a given probabilistic tsunami hazard analysis (Chock et al. 2016).

Research Objectives

This research aimed to add to the existing literature by developing a novel test setup to measure the internal and external demands on a scaled structural system and use the results to validate a model that can be utilized for CFD analysis of structures subject to coastal inundation events such as tsunamis. The model can assist in the evaluation of demands in new parameter spaces, including the numerical simulation of tsunami-like bores impinging against structures at full scale, something that may be of great use to the natural hazard and risk and resilience communities. The research involved four distinct phases. The phases were as follows: (1) an evaluation of existing standards for determining appropriate demands for a representative vertical evacuation structure; (2) an experimental investigation of a 1:6-scale prototype specimen of a representative VES concrete core wall lateral force resisting system; (3) a numerical investigation involving a CFD model of the 1:6-scale experiments to demonstrate the efficacy of utilizing modeling to predict the hydrodynamic forces of wave impingement upon a structure; and (4) an evaluation of predictions from existing standards to results extrapolated at similitude from experiments to full scale and associated discussion.

The experiment was first modelled to investigate the impact of the beach slope and location on the demands to design the bathymetry for the experimental study, as well as to determine the appropriate placement of instrumentation. The experimental investigation was designed to measure the demands on a 1:6-scale structural prototype core-wall model that included a pile foundation using a large wave flume and extensive instrumentation, including pressure sensors, strain gauges, and a series of load cells to measure all base reactions. The prototype model included the structural and foundation systems and coarse methods of capturing the boundary condition provided by the soil. The experimental study investigated the influence of wave breaking and soil height on the demand. After experimentation, the numerical modeling approach was validated by comparing the numerically simulated and experimentally measured demands, including wave velocity, pressure distribution, and reaction forces, to develop recommendations for computational fluid dynamics (CFD) modeling. This involved applying boundary conditions to the numerical model that correlated with the experimentally measured values, particularly the wavemaker paddle movement at the anterior end of the flume. Following the validation of the numerical and experimental results, codified predictive equations were evaluated. The correlated numerical and experimental results were scaled using Froude number similitude laws and compared to ASCE codified design equations for tsunami inundation forces due to a flow at an equivalent height to the similitude-scaled experimental values.

Literature Review

Significant research investigating tsunami or tsunami-like waves on structures has been conducted over the last three decades, with advancements in probabilistic, experimental, and numerical simulation methods. Small scale tests have shown that load cells work well to provide a realistic fixed boundary condition at the base of a structure when testing structures against tsunami-like events in laboratories. However, when structures become larger and heavier, additional restraints may be required for stability or load isolation, complicating the accurate measurement of force (Wienke and Oumeraci 2005). Without a load cell or pressure sensors in the main direction of loading, it may be impossible to resolve the base shear imparted to a structure accurately (Wilson et al. 2009). Demands from wave and tsunami-like bore impact can be measured or validated with load cells and pressure sensors on the front face of a test specimen (Shafiei et al. 2016). For larger specimens, multiple pressure-sensor layouts can be used and integrated to capture the pressure distribution over the front face (Gills 2018).

A statistically dependable methodology for determining the overall magnitudes of force that can be imparted to structures from tsunami wave impacts is the ASCE 7-16 minimum design loads and associated criteria for buildings and other structures (ASCE 2017). These provisions offer a conservative estimate of fluid-induced forces using the fundamental physics of hydrostatics and hydrodynamics; they are experimentally validated and were built upon decades of research into tsunami inundation events and their impacts upon structures within their region of effect. The demand equations and design provisions are intended to improve both tsunami resilience and the overall life safety of coastal communities and their buildings (Chock et al. 2013, 2018; Chock 2016; Foster et al. 2017). Although the magnitude of the force imparted to structures from tsunamis at a global scale can be determined using equations such as those provided by these provisions, this simplified analysis tells us nothing about the local forcing effects upon a structure, nor do they tell us anything about the load flow of the full load from the structure to the ground. Nonlinear static pushover analysis of structures subject to tsunami loading has been conducted in studies such as Baiguera et al. (2019, 2022), Rossetto et al. (2018, 2019) studied the postearthquake resilience of structures subject to tsunami loading. However, these studies were limited in that their consideration of the postyield effects of structures cannot account for second order effects due to fluid bearing or dynamic impact or intrusion of fluid within a building perimeter after impingement of a tsunami against the facade or glazing of the structure. However, analysis and design techniques such as those cited in this section are state of the art and are considered to be the most comprehensive methods available for performance-based tsunami resilience engineering.

In cases of experimental or theoretical uncertainty, integrated numerical/experimental validation studies can provide confidence in both numerical and experimental results whose accuracy is questionable due to experimental and numerical variability and error; such studies have a long history in the field of aerodynamics and aeroelasticity. Examples of integrated computational/experimental studies go as far back as the 1980s, in which CFD predictions were utilized by US National Aeronautics and Space Administration engineers to determine wind tunnel testing parameters and estimate drag and lift forces and pitching moments (Melton et al. 1989). Such studies, when performed properly, provide researchers with the means to both predict and extend results from experiments. Preliminary numerical analysis can aid in the design setup and determination of testing parameters for experimentation to allow for expedited testing schedules and can also provide baseline expected responses of a test system. Measured values from experiments can then be cross-validated with preliminary simulations, and simulations and data therefrom can be used to advance the CFD models by comparing the experimental and numerical results. Once validated, a model can provide data that cannot be measured, thereby advancing the understanding of the demands and system response. For example, Motley et al. (2016) investigated bore-type tsunami loading on a model bridge at various skew angles numerically and experimentally to examine the effect of skew upon the nature of the

force time histories imparted against the bridge. They found that bore impact forces on skewed decks occur in different directions over time, often one direction immediately after another, including pitching and spinning moments. The nature of these forces can lead to increased horizontal reactions in substructure components, resulting in the unseating of a bridge deck. This investigation also included a CFD study of the experimental setup that showed a strong correlation between forces calculated by the numerical model and the measured values from experiments. Similar studies of wave-induced forces against structures that demonstrate the use of CFD as a predictive tool for wave-induced forces and as a verification and validation tool for experimentally acquired data include Seiffert et al. (2015), Xiang et al. (2020), Winter et al. (2020), and Yang et al. (2021).

Experimental Investigation

Representative Vertical Evacuation Structure

Using ASCE 7-16 to determine both site-specific earthquake and tsunami demands, a representative vertical evacuation structure containing concrete shear core walls was designed to remain linearly elastic under design loads. All calculations for the demands and the design of the representative vertical evacuation structure can be found in Chapter 3 and Appendix A of Pyke (2020). An abridged summary of these calculations is provided here for reference. Seaside, Oregon was selected as a potential site to place the evacuation structure. The region was examined in prior research projects to determine potential tsunami inundation depths within the city, and for simplicity, a site was chosen somewhere within the region for which experimental modeling had already been completed at reduced scale (Rueben et al. 2011) and numerical modeling had been carried out at full scale (Qin et al. 2018). A building footprint with exterior dimensions of 45.720 m × 18.300 m with a height of 22.860 m (5 stories total, with a story height of 4.572 m) was selected. A floor plan of this representative vertical evacuation structure is shown in Fig. 1. Initial sizing of the proposed structure led earthquake loading from ASCE 7-16 provisions to be of significantly greater magnitude than tsunami loading. As an academic exercise, the building was sized in width perpendicular to the inundation flow such that the codified earthquake and tsunami forces were approximately equal. This was completed by iteratively reducing the width of the structure subject to incoming flow from tsunami inundation, which reduced the seismic weight of the structure and, in turn, reduced the expected magnitude of earthquake forces. The premise of this exercise was to develop a lateral force resisting system for earthquake induced forces and to investigate the effects of tsunami-generated forces upon a system designed solely for seismic effects. In practice, this may not be a direct approach; this will depend on local site conditions related to both local seismic and tsunami hazards. The structure contained three concrete shear wall cores, one at each end of the 45-m side of the building on opposing corners and one near the center of the floor plan. The structure's design was intended to ensure that the upper levels were capable of being used for evacuation during a tsunami. If nonessential walls beneath the evacuation structure were capable of washing away in an inundation event, the amount of force imparted to the structure as a whole could be minimized. The upper levels of the structure would house essential facilities and serve as an evacuation shelter. Functions for this sacrificial first story of the building could include lobby space, parking, retail, or other open shared spaces that

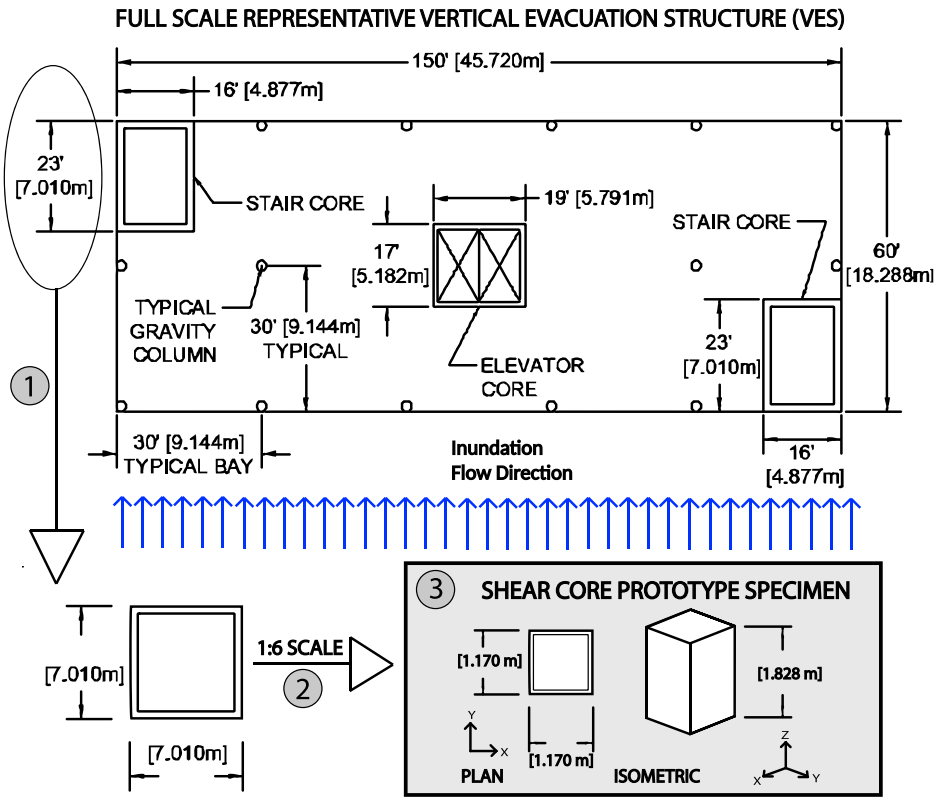

Fig. 1. Floor plan of representative full scale vertical evacuation structure. From this design, the prototype specimen which was utilized in testing and numerical analysis was developed. (1) The longest wall of the shear core system was taken and made into a square; (2) the square was scaled down to 1:6 of original size; and (3) the prism was shortened to 1.83 m in height to fit within the test facility.

J. Struct. Eng., 2022, 148(12): 04022200

are unlikely to be occupied during a multihazard event. Assuming that a 0.254-m-thick, two-way, reinforced concrete slab with mild reinforcement (7.18 kN/m^2) was used as the floor system at each level including the roof, a seismic weight of 1,530,900 kg per story was determined. Using the equivalent lateral force (ELF) procedures detailed in ASCE 7-16 and the site-specific accelerations from a given maximum considered earthquake (MCE) event for the chosen structural properties and estimated building period, the overall design base shear imparted to the full scale representative VES from an earthquake that could precede a tsunami was found to be 56.2 MN. Tsunami loads were calculated using inundation heights and fluid velocities obtained from the energy grade line (EGL) method detailed in ASCE 7-16, Chapter 6, Section 6.6. This method calculates inundation depths and flow velocities at a specific location, taking into account energy losses in the tsunami from changes in elevation and surface friction along the ground using topographical data from the tsunami run-up trajectory. The largest inundation depth and flow velocity at the building site were 8 m and 8.9 m/s, respectively. Using the equations in ASCE 7-16 Section 6.10, assuming that a uniform pressure acts over the face of the structure that is closest to the shore, the tsunami load for the whole structure was estimated to be 65.7 MN. Tsunami loading was the controlling load case for the onshore direction (perpendicular to the 45.7-m side of the building), while earthquake loads were the controlling load case for the direction parallel to the shore. Earthquake and tsunami forces were distributed to the multiple shear cores of the overall structure based on the ratios of the stiffness values of the different core wall systems to the overall structural stiffness, acting as the load transfer mechanism for the lateral forces to the ground. The core walls and their reinforcement were then detailed to fully resist the design earthquake and tsunami loads while remaining linearly elastic.

Prototype Test Specimen

From this representative VES, a prototype concrete core shear wall test specimen was developed by scaling down the design of the full-scale lateral force resisting system (LFRS) from the representative vertical evacuation structure to meet the dimensional constraints of the experimental facility. More specifically, the geometry of the specimen was designed by taking the longest wall of the LFRS shown in Fig. 1, the 7-m side of the exterior core wall, and making a square box. At the scale possible within the flume (1:6 scale) this translated to a test specimen that was 1.168 × 1.168 m with 0.127-m-thick walls. In order to cut down on weight, the height of the specimen was reduced to 1.830 m. The specimen also had a 0.165 m slab at the base of the walls, representative of a structural slab that would transfer lateral loads to the substructure. The slab thickness of the 1:6 prototype specimen was dictated by how large it would need to be to fit rebar with appropriate dimensions (clearances, bend radius of bars, cover, etc.). The width of the specimen was designed to allow sufficient space between the flume wall and the specimen to permit water to flow around the structure freely, maximizing the clear distance and allowing for a 1:6-scale model, permitting use of actual structural materials. Number 4 reinforcing bars were placed in the specimen, with a reinforcement ratio of 0.02 in each direction. Based on the loads applied to the specimen from preliminary modeling, the concrete was not expected to crack under wave loading. To avoid consolidation issues in the 12.7-cm-thick walls with 2 curtains of rebar, a 9.5-mm pea gravel concrete mix with a high slump was used.

This rectangular concrete core specimen sat on four piles embedded into the corners of the walls and the base of the soil box, supporting the core and its slab when there was no soil beneath. Foundation pile sizing was determined using the largest possible commercially available steel tube that could fit into the walls of the shear core between the curtains of reinforcement. No specific calculations were completed in design of the piles other than to check that they would not buckle under the weight of the specimen. The steel tube casing of the pile acted as both a confining and tension element for reinforcement of the concrete matrix, precluding the need for additional rebar within the pile. The lengths of the piles were chosen to allow the bottom of the specimen to meet the bathymetry of the flume at the height desired with the soil box assembly beneath it. After reinforcement was placed, the steel tubes used for the piles were placed inside the rebar cage and run to 2 cm from the top of the specimen's walls.

The specimen atop its piles was located within a 2 × 2-m steel and concrete box containing gravel, representing soil. This soil box was intended to allow for the effects of the presence of soil around the foundation piles upon structural response to be investigated, which would offer some information about changes in the performance of the structure if it were subjected to scour of the soil around the foundation. To investigate the effects of the removal of soil on the load transferred from the piles to the soil, the tests were completed with the soil box filled to various levels, with the soil box covered by impermeable floor panels. The floor panels were intended to protect the specimen's soil from uncontrolled scour and to allow for the same soil conditions to be in place for repeated wave impact trials by preventing removal of the soil from the box. While this did not capture the progression of scouring around the structure, it did provide a physical representation of various levels of scour. Steel walls were attached around the edge of the concrete base to make the sides of the soil box and support the floor panels. The specimen's piles were cast at their lower end into the concrete base, which formed the bottom of the soil box and acted as a load transfer diaphragm from the piles to the load cells. Pea gravel was selected as the representative soil because it was readily available at Oregon State University (OSU) and was not likely to be removed from the soil box by wave action; mixes containing sand and other aggregates of smaller diameter were not permitted during testing. The specimen's foundation piles were embedded in 0.99 m of compacted soil when the box was completely full. The soil box was attached to a series of pin–pin connected load cells, which themselves were attached to the flume walls and floor via a reaction frame. The reaction frame consisted of two W12×106 beams running parallel to the length of the flume. These beams had another section welded upright to them in order to connect the streamwise load cells. Two other W12 × 106 beams were placed transversely over the lower beams, and the assembly was tensioned to the floor of the flume. Specimen design, construction drawings, and more information about the development of the experimental procedures utilized are described in detail in Appendix B of Pyke (2020).

Test Setup and Instrumentation

The dimensions of the specimen and the test set up, including instrumentation, is shown in Fig. 2. This complex setup was used to support the soil box from below and the sides to restrain the structure while measuring reactions in three primary directions—vertical forces, transverse forces (forces perpendicular to the length of the flume), and streamwise forces (forces acting parallel to the length of the flume). A variety of instruments, including load cells, pressure sensors, and strain gauges, facilitated redundant measurements and validation for base shear and overturning moment.

An instrumentation bridge spanned across the flume above the specimen, allowing for the measurement of water surface elevation

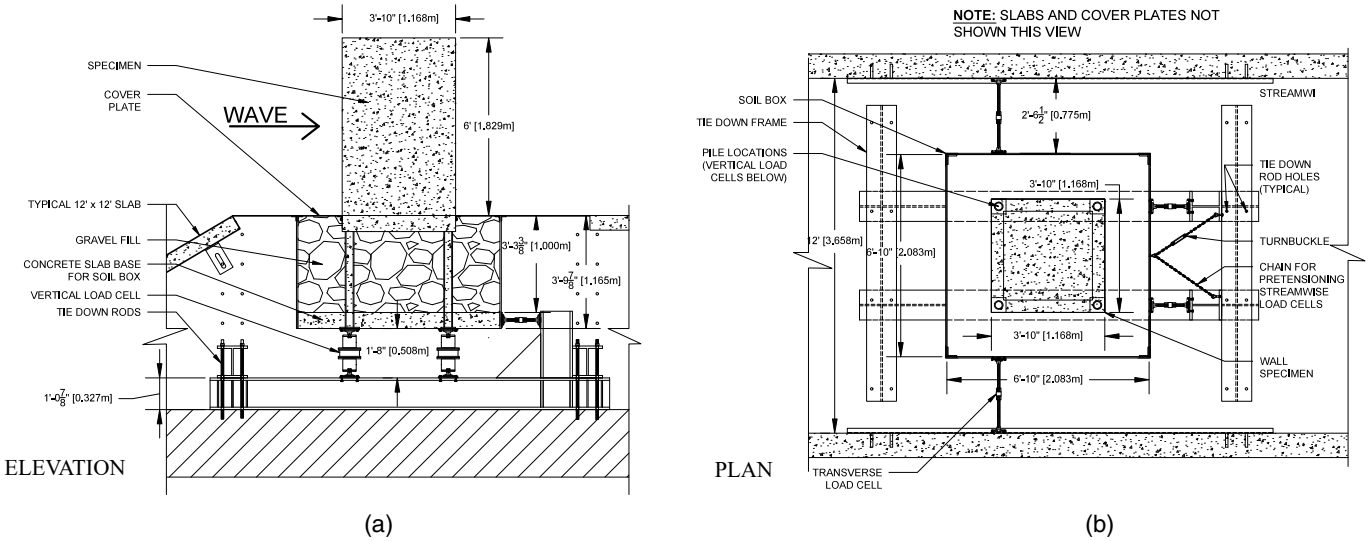

Fig. 2. Specimen dimensions.

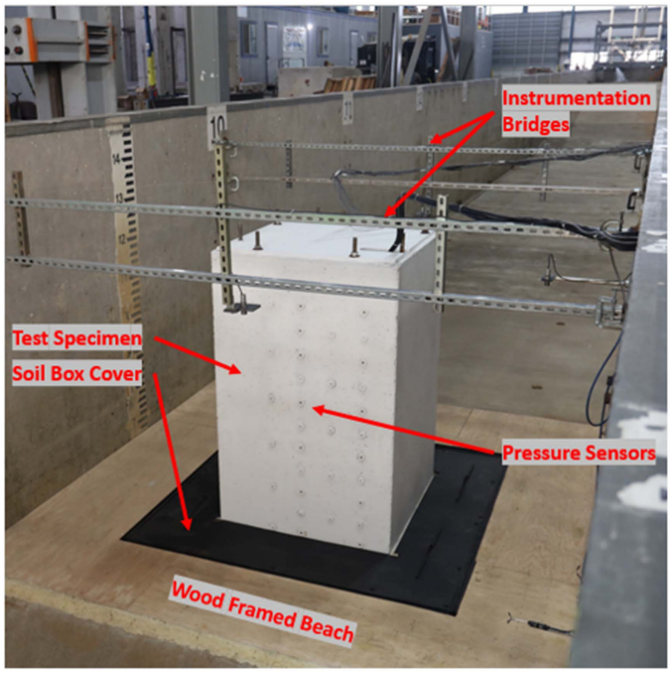

Fig. 3. Specimen in testing configuration.

around the wave impact zone by means of ultrasonic wave gauges. This instrumentation bridge and the pressure sensors on the upstream face of the specimen are shown in Fig. 3. Multiple wire resistance wave gauges were used to record free-surface elevations from the tests at points specified in Fig. 4 along the length of the flume; these measurements were compared more closely with the CFD model. Fluid velocities were measured using acoustic Doppler velocimeters (ADVs) located at points along the flume near the test structure, as shown in Fig. 5. The exact geometric locations, trial counts, and coefficients of variation of the wave gauges, ADVs, and pressure sensors utilized in this study are listed in Table 1. USWG 3 and USWG 4 were not used in comparison or for data analysis due to excessive noise caused by water droplets splashing on the sensors from the mist generated by wave impingement on the bathymetry. Data from ADV 4 was omitted due to a lack of discernible information obtained from the sensor, because the noise magnitude at the onset of inundation of the ADV was too great to measure accurate velocities from the instrument.

Streamwise forces were measured using two rod end load cells connected to the back end of the soil box and to the base reaction frame. Uplift and overturning forces were measured by four pancake-type load cells attached to the bottom of the soil box. Transverse load cells were secured to channels attached to the flume walls on either side of the specimen. Each load cell connection consisted of a swivel at both ends that allowed the load cells to only carry axial compression and reduced the interference between load cells oriented orthogonally. Moments were calculated by multiplying each load cell's contributions to the global reaction force by the moment arm from the center of the load cell to the center of mass of the structure.

Shear and axial forces from specimen response were measured using strain gauges attached to concrete-filled tubes (CFTs) acting as piles; these were located within the soil box below the specimen. Four strain gauges were located along the height of each concrete-filled tube foundation pile, near the bottom and top of both the front and back of each pile. Exact locations of the strain gauges are shown in Fig. 6. Axial forces were easily calculated from the shortening of the strain gauges and the axial section properties of the piles, but calculating shear forces required first calculating the curvature of the

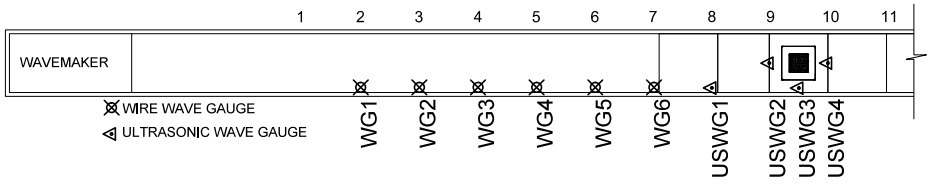

Fig. 4. Wave gauge locations.

J. Struct. Eng., 2022, 148(12): 04022200

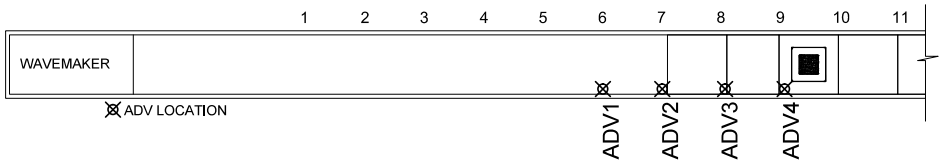

Fig. 5. ADV locations.

Table 1. Instrument locations

Instrument	x-position (m)	y-position (m)	z-position (m)	No. of trials	Coefficient of variation (%)
WG1	13.96	−1.39	1.33	20	0.9
WG2	17.6	−1.39	1.32	20	1.4
WG3	21.28	−1.39	1.31	20	1.8
WG4	24.93	−1.38	1.32	20	2.9
WG5	28.59	−1.38	1.32	20	4.1
WG6	32.24	−1.38	1.32	20	4.4
USWG1	36.04	−1.38	3.63	20	1.6
USWG2	39.97	−0.03	3.82	20	2.3
ADV1	28.57	−1.45	0.92	20	0.6
ADV2	32.22	−1.45	0.93	20	1.3
ADV3	36.08	−1.46	0.93	20	19.6
A01	40.77	−0.20	1.52	10	9.0
B01	40.77	0.00	1.52	10	15.0
D01	40.77	0.39	1.52	10	5.0
C06	40.77	0.20	0.76	17	6.0
B06	40.77	0.00	0.76	10	1.0
D06	40.77	0.39	0.76	10	1.0
A11	40.77	−0.20	0.02	17	2.0
B11	40.77	0.00	0.02	37	2.0
D11	40.77	0.39	0.02	10	1.0

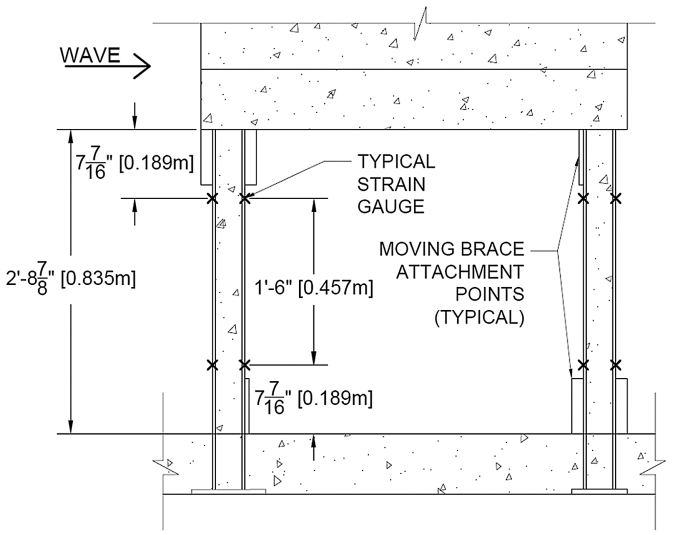

Fig. 6. Strain gauge locations.

concrete-filled tube section at each instant in time at eight stations with strain gauges at both external fibers, two for each pile. The moments calculated at these eight points from the section properties and curvatures were then used to calculate shear forces within the piles. Overall specimen shear forces, axial forces, and moments were computed by summing forces at known stations about the specimen's center of rigidity, which was presumed to be at the center of the base of the concrete portion of the specimen.

Thirteen pressure sensors were used to characterize the pressure distribution over the front face of the wall. They were placed in different layouts over several trials in order to fully capture the surface pressure field characteristics. Five different pressure sensor layouts were used. These pressure sensor layouts were used together in various trials to determine an interpolated pressure distribution over the upstream face of the specimen, which was then integrated to obtain the applied force. This force was compared to the measured forces from both the load cell and the strain gauge resultants. Pressure sensors were labeled numerically and spaced equally along vertical grid lines—the locations of each pressure sensor in each layout was mapped to its grid location on the wall. The exact locations of the pressure sensors on the upstream face of the specimen are shown in Fig. 7.

The purpose of utilizing load cells, strain gauges, and pressure sensors collectively for determination of base shear was to investigate the overall behavior of the system as it sat in situ. Pressure measurements allowed for the determination of applied forces on the upstream face of the specimen; strain gauges in flexural members (foundation piles) allowed for the measurement of the response during loading; and load cells placed beneath and behind the foundation allowed for an understanding of the total load applied to the instrumented subassembly. Unfortunately, the load cells picked up load from the region surrounding the specimen as well as the specimen itself, resulting in large inaccuracies with respect to the measured values for vertical force obtained from strain gauges. These discrepancies are addressed in the following section.

During all testing, a National Instruments (Austin, Texas) PXI architecture data acquisition system (DAQ) was used. Data were sampled at a rate of 100 Hz. In total, 51 channels were used to collect data from the 13 pressure sensors, eight load cells, 16 strain gauges, four ultrasonic wave gauges, six wire wave gauges, and gauges in the wave maker that determined its displacement, water level in front of the paddle, and motion start time. A separate DAQ was synchronized to collect data for the ADVs, because they required a special proprietary software to change their signal into usable velocity data.

Test Facility

The 1:6-scale VES prototype was tested in the large wave flume (LWF) at the Hinsdale Wave Research Laboratory (HWRL) at OSU. The LWF is 104.0 m long, 3.7 m wide, and 4.6 m deep. Waves are generated by a piston-type wavemaker on the upstream end of the flume. The wavemaker at HWRL is capable of producing any user-defined wave capable of being generated within the physical constraints of the motion of the pistons with a provided still water level. Its maximum stroke is 4.0 m with a maximum velocity of 4.0 m/s. The maximum still water level (SWL) in the flume that a wave can be generated in is 2.0 m. The maximum stable wave height the facility is capable of creating given these constraints is a 1.40-m solitary wave. Unstable waves can be produced by generating waves of taller height than this; such waves then break and propagate as a turbulent bore.

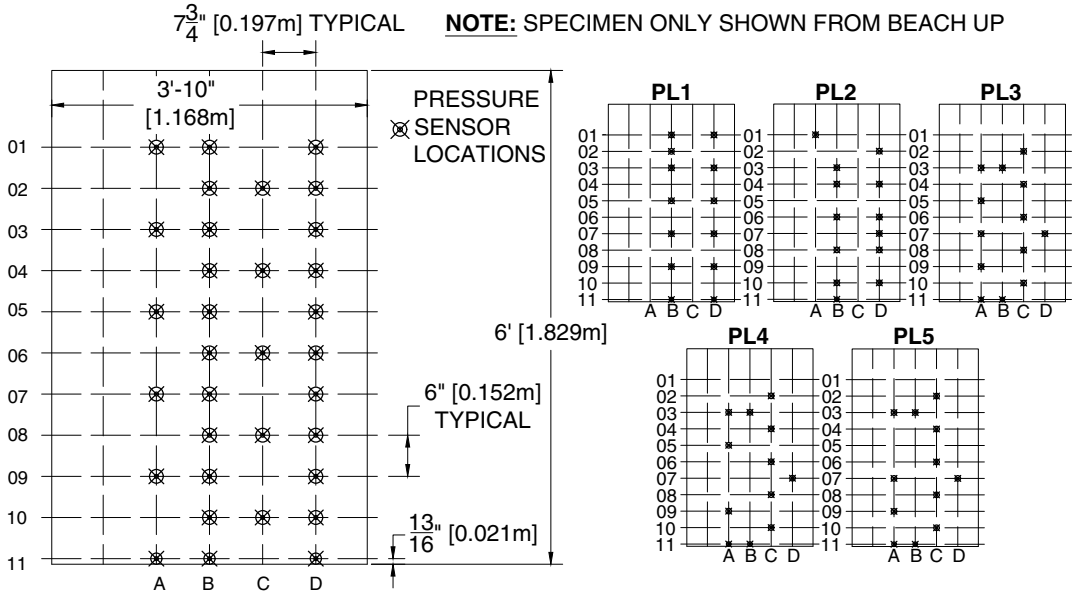

Fig. 7. Pressure sensor locations.

To provide an adjustable flume bathymetry, a set of 0.15-m-thick, 3.66-m-square movable concrete slabs were used as the flume bed. The flume bathymetry used in this study consisted of a submerged horizontal bottom section starting at the wavemaker followed by a sloped beach and dry horizontal sections formed by the movable slabs. To determine what bathymetry slope and wave height would produce the largest force on the test specimen, a series of preliminary analyses were performed using a numerical model of the flume. This modeling was also used to determine the approximate forces that would act upon the test specimen in order to design the test setup. A parametric study on the test specimen location and bathymetric slope was completed to determine where the structure should be placed in the flume and what slope should be used to achieve the largest possible wave and wave force. The model utilized was the same height and width as the LWF at OSU. A description of all variables and model information is available in the model description section.

Ramp slopes of 1:1, 1:2.5, 1:5, 1:10, and 1:15 were simulated, while the ramp location was varied. The distance from the wave maker neutral position to the top of the ramp was changed from 20 to 70 m in increments of 10 m to investigate best location of the beach for development of the wave. For each possible combination of ramp slope and distance, a 1.40-m solitary wave was generated in 2 m of still water by the wave maker; the calculated free surface height at the top of the ramp, obtained from preliminary simulations at the location of ultrasonic wave gauge USWG2, was recorded. It was found that the steeper the slope of the ramp, the larger the wave generated at the top of the ramp. From this study, it was decided that a ramp with a slope of 1:1 should be used and the specimen should be placed as close to the wave maker as possible. To avoid having to build a custom slope, the ramp slope chosen for the experiments was 6.56:10 or 33.1, with a height of 2 m, because the LWF utilizes precast concrete slabs with a length of 3.66 m to create bathymetries in the flume. Upon discussions with staff from the LWF, it was decided that the structure should be placed between bays 9 and 10 in the flume, approximately 40.77 m from the neutral position of the wave maker. This gave the waves time to fully develop after generation and provided room to place wave instruments before the slope to help characterize the wave. The position of the specimen within the flume, with dimensions, is shown in Fig. 8.

Two wave types of nearly identical time scale were utilized in this study ($T \approx 2.25$ s). The first wave type is referred to as the 1.40-m wave, and can be classified as an unbreaking solitary wave. The second was slightly taller and is referred to as the 1.45-m wave; this wave broke almost immediately after forming. This wave approached the structure as a broken bore and can be characterized as a spilling breaker wave. These two waves of similar height were chosen to investigate the effects of the turbulent bore of the broken wave upon the forces imparted to the specimen. Tsunami events often involve multiple waves, but they show up individually

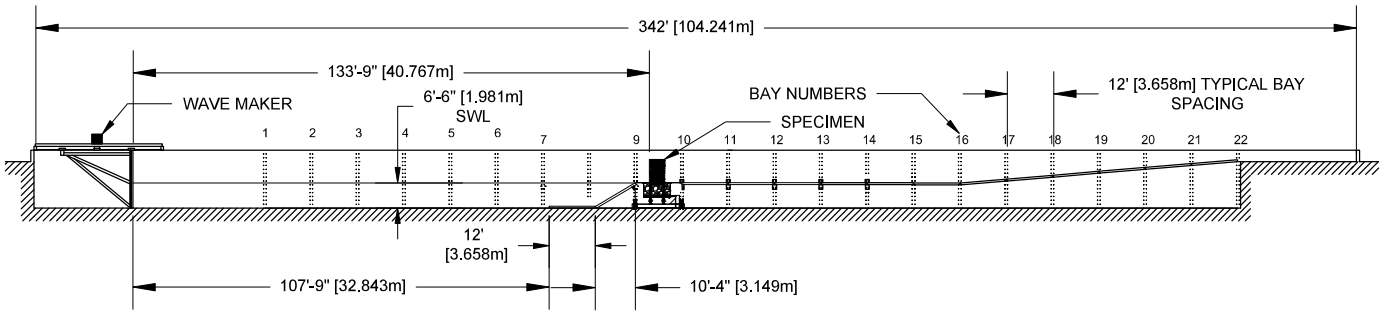

Fig. 8. Specimen location in flume.

J. Struct. Eng., 2022, 148(12): 04022200

Table 2. Experimental test matrix: number of trials for each soil condition

Wave height (m)	1.40			1.45
Soil condition	E	H	F	E
Trials	30	35	37	20
PL1	10	10	10	5
PL2	10	10	10	5
PL3	10	10	10	5
PL4	0	5	0	0
PL5	0	0	7	5

Note: E = empty; H = half full; and F = full.

with gaps in time between their occurrence. While the flume is not capable of generating a true tsunami wave, the facility represents the state-of-the-art in the experimental wave loading of a structure. In order to reproduce the turbulent bore flow characteristics of a tsunami inundation within the flume, breaking waves were created by generating a solitary wave that then propagated along the flume until it broke due to flume bathymetry variations or its own initial height. With respect to the nature of the waves studied, while spilling breaker and unbroken solitary waves are not exact when it comes to modeling the effects of tsunamis at scale (Madsen et al. 2008), the methodology utilized in this experimental study was the best available science to the authors and has been used previously in studies investigating tsunami effects at scale (Robertson and Mohamed 2009; Swigler 2009; Lynett 2009). However, caution should be taken when extrapolating results from this study and others utilizing solitary waves to determine the behavior of structures subjected to tsunami loading, because the time scales of the waves utilized in this study and those of true tsunamis vary greatly.

Experimental Results

The experimental study parameters and the number of trials associated with each parameter are documented in Table 2. Three experimental phases were conducted with a wave height of 1.40 m; one experimental phase was conducted with a wave height of 1.45 m. For each experimental phase, a minimum of three pressure sensor layouts were required to fully characterize pressures across the front face of the specimen. For the first experiment, the 1.40-m wave with the soil box full, 10 trials were run for each pressure sensor layout to ensure repeatability of the pressures. The specimen was tested with the soil box full, half full, and empty in order to investigate how loss of soil around the piles affects load transfer and loss of restraint and stiffness. Based on the results from our experiments and the absence of a noticeable difference between forces measured from the various soil conditions, it is believed that the soil box was not large enough for the presence of soil to have any effect on the motion of the piles by means of a confining force. The trials involving the 1.45-m wave were run only with the soil box empty, because the soil level was shown to have little, if any, effect on the measured forces. Due to the consistency of pressure measurements between trials for the 1.40-m wave height, experiments were run with only five trials for each pressure layout for the 1.45-m wave height. Overall, a total of 30 trials were run for the 1.40-m wave with the soil box empty, 35 trials were run for the 1.40-m wave with the soil box half full, 37 trials were run for the 1.40-m wave with the soil box empty, and 20 trials were run for the 1.45-m wave with the soil box empty.

Peak forces and moments in all directions for each study parameter are listed in Table 3. Peak streamwise force was computed in multiple ways, using load cells, strain gauges, and through the integration of pressure sensors by means of a linear interpolation between the locations of the pressure sensors. Pressures measured along the height of the wall on the streamwise face were reflected about the centerline of the specimen, then mapped to a discretized grid over the entire face. Integration over the discretized grid utilizing linearly interpolated pressures was then completed to resolve the applied force to the upstream face of the specimen from the pressure sensor measurements. For a wave with a maximum crest height of 1.45 m and a celerity (the velocity with which a wave advances) of 5.82 m/s, the structure experienced forces near 30 kN in the streamwise direction, with an overturning moment of over 20 kN·m in the pitching direction. These are among the largest forces that can be generated in the flume for a still water level of 2.0 m. With just a slightly larger wave height, forces from the 1.45-m wave case were considerably higher than those of the 1.40-m wave. It is assumed that this was due to the turbulent bore developed by the spilling breaker wave produced by generating an unstable wave height of 1.45 m.

Floor panels spanning from the edge of the soil box to the face of the specimen took vertical force from the water bearing upon the panels near the specimen as the wave passed by. These forces were measured by the load cells located under the soil box directly beneath the specimen's foundation piles. The location of the flooring from which the additional forces originated can be seen in Fig. 3 as black regions near the base of the structure. Forces in the streamwise direction from the impact of the waves against the flooring surrounding the specimen were transferred through the soil box and measured by load cells positioned downstream from the specimen, resulting in a discrepancy in forces in the streamwise direction between the load cell and strain gauge resultants.

A small asymmetry in either the placement of the specimen within the flume or the stiffness of the instrumentation assembly holding the specimen resulted in slight rolling and yawing moments upon the specimen about its minor axes of rotation as well as translation reaction forces associated with these actions. This can be seen

Table 3. Peak forces and moments by study parameter

Wave height (m)	Measurement origin	Soil box condition	Fx (kN)	Fy (kN)	Fz (kN)	Mx (kN·m)	My (kN·m)	Mz (kN·m)
1.40	Pressure sensors	Empty	23.46	N/A	N/A	N/A	N/A	N/A
1.40	Strain gauges	Empty	23.04	0	8.83	1.25	20.5	2.01
		Half full	21.01	0	8.46	1.33	18.26	2.07
		Full	22.25	0	7.43	3.53	19.67	1.86
1.40	Load cell	Empty	32.43	0.42	104.17	0.69	17.01	1.94
		Half-full	32.44	0.43	105.36	0.75	16.92	1.94
		Full	32.47	0.42	105.54	0.54	17.19	1.94
1.45	Pressure sensors	Empty	25.91	N/A	N/A	N/A	N/A	N/A
1.45	Strain gauges	Empty	25.74	0	11.13	2.28	24.31	0.41
1.45	Load cell	Empty	37.62	0.61	106.09	0.8	22.41	2.57

Note: Fx = streamwise; Fy = transverse; Fz = lift; Mx = roll; My = pitch; and Mz = yaw.

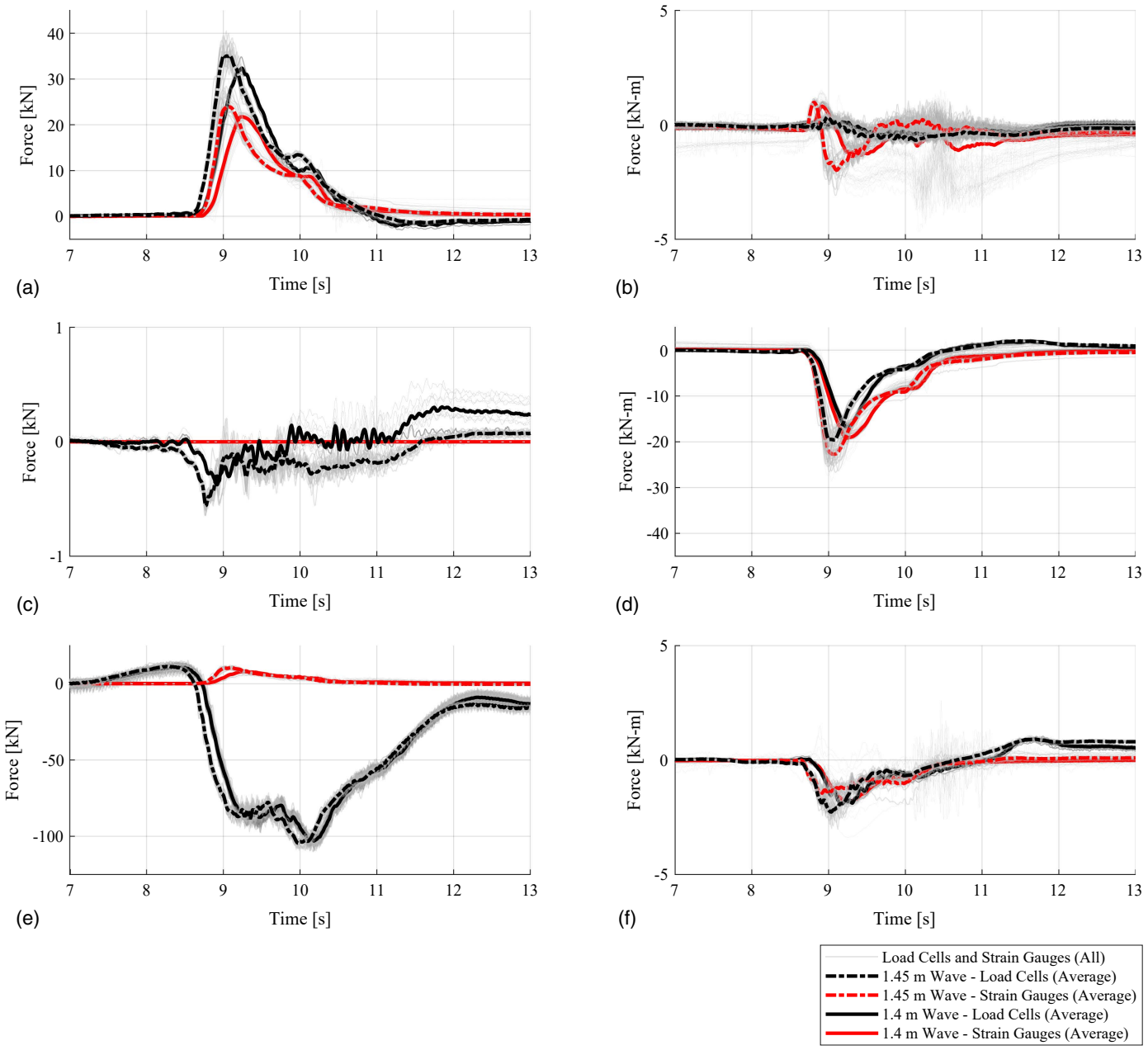

Fig. 9. Wave impact forces—all trials (gray); and trial averages from 1.40-m (solid) and 1.45-m (dashed) wave height sequences—force comparison between load cell measurements and strain gauge measurements: (a) streamwise force; (b) roll moment; (c) transverse force; (d) pitch moment; (e) vertical force; and (f) yaw moment.

in the upper- and lower-right panels of Fig. 9. The specimen first experienced a force in the positive roll direction when the wave initially struck, then a reversal of the sign of the moment back to the negative direction as the wave bore rolled around its sides. In this instance, the soil box appeared to experience a slight transverse force (<0.5 kN) associated with this rolling moment and its effects on the flow around the structure.

Numerical Investigation

The following section presents the investigation into the efficacy of CFD in simulating wave–structure interactions from paddle-generated breaking solitary waves and the resolution of experimental forces for integrated study of fluid behavior using a model at 1:1 scale with the experiments.

Model Description

Numerical analysis and modeling was completed using CFD with the open-source Field Operation and Manipulation (OpenFOAM version 7) (Weller 1998) software package. OpenFOAM is a collection of C++ libraries that can be compiled to create individual applications, which are broadly categorized as either solvers or utilities. The cases examined here were simulated using the olaFlow solvers (Higuera 2018), an open source project developed within the OpenFOAM framework that solves the three-dimensional volume-averaged Reynolds-averaged Navier-Stokes

equations (VARANS) using finite volume discretization; this allows the simulation of physically correct two-phase incompressible fluid wave generation and active wave absorption.

The two incompressible phases (water and air) were tracked using the volume of fluid (VOF) technique to represent complex free surface configurations (Hirt and Nichols 1981). An indicator function α was defined for the volume fraction of the two-phase fluid; it had a value of 1.0 corresponding to regions occupied by one phase, in this case water ($\rho = 1{,}000\ \text{kg/m}^3$, $\nu = 1.0 \times 10^{-6}\ \text{m/s}^2$), and a value of 0.0 for the other, in this case air ($\rho = 1.22\,\text{kg/m}^3$, $\nu = 1.48 \times 10^{-5}\ \text{m/s}^2$), where ρ = mass density of the fluid; and ν = kinematic viscosity. Intermediate values indicate cells that contain a mixture of water and air, for which the free surface between the fluids is not resolved explicitly. When free-surface tracking was necessary in this study, a volume fraction of 0.5 was used to identify an approximate free surface. The α field was initialized at a still water level of 2 m to match the free surface of the water at rest in the experiments.

The k-ω shear stress transport (k-ω SST) model was utilized for the modeling of turbulence. The k-ω SST model, described by Menter et al. (2003), models turbulent kinetic energy k, turbulent kinetic energy dissipation rate within the boundary region ω, and turbulence viscosity ν_t. This turbulence model formulation captures the turbulent kinetic energy generation in the near field of the wall much better than k-ϵ models, resulting in higher fidelity of shear stresses and forces imparted upon objects or structures within the flow. The variable ϵ in these equations represents rate of dissipation of turbulent kinetic energy farther away from the boundary. The k-ω SST model is essentially an extension of k-ϵ models, with almost identical behavior of the k-ω SST model and k-ϵ models far away from boundaries; however, the authors found that slightly better results for viscous shear were generated near structures with the k-ω SST model. The turbulence model was initialized with the following values for turbulence coefficients: $\text{k} = 9.54 \times 10^{-3}$, $\epsilon = 4.45 \times 10^{-4}$, $C_\mu = 0.90 \times 10^{-1}$, and $\omega = 0.52$.

Model dimensions can be seen in Fig. 10. Atmospheric boundary conditions for variables U (velocity) and p_{rgh} (dynamic pressure) were applied to the topmost boundary of the model. All walls except the atmosphere boundary were assigned standard wall boundary conditions for the simulation. Specific boundary condition types for the turbulence model and dynamic mesh library were applied to necessary regions of the model for initialization of mesh movement and satisfaction of the requirements for numerical stability. Waves were generated by a pneumatically powered piston at one end of the wave flume and then propagated down the length of the flume to a sloped bathymetry, forcing the waves to initially spill and then fully break, resulting in a turbulent bore prior to the flow reaching the test structure.

In order to replicate the experimental wave motion and measured fluid loads imparted on the structure, the displacement of the paddle during experiments was recorded as a time history. This paddle displacement history was imposed on the wavemaker paddle surface in the OpenFOAM model using the olaFlow boundary condition function wavemakerMovement to specify the mesh motion. More specifically, mesh-morphing wave generation boundary conditions were used to mimic the piston-driven paddle wavemaker at the Hinsdale Wave Research Laboratory by prescribing the variable pointDisplacement within OpenFOAM. All boundary conditions applied in the models are listed in Table 4. For further information and a comprehensive evaluation of OpenFOAM boundary conditions used in large wave flume models such as those utilized in this study, see Winter (2019). The computational domain was comprised of 3.2 million points and 3 million cells, with cell sizes varying from $10 \times 10 \times 10$ cm, far from the structure, to $1.5 \times 1.5 \times 1.5$ cm, near the structure. Time discretization was initialized with a 1×10^{-4} maximum and 1×10^{-9} minimum time step, with time step size governed by a Courant Friedrichs Lewy condition of 0.5. The models were run on 28 processors, with 128 GB of memory per processor, and took approximately 50 h to complete.

Computational Results

The simulated results for wave movement, pressure distribution over the specimen, and structural forces were compared against the measured responses to evaluate the accuracy of the model. Fig. 11 shows elevation views of the simulated wave at various points of

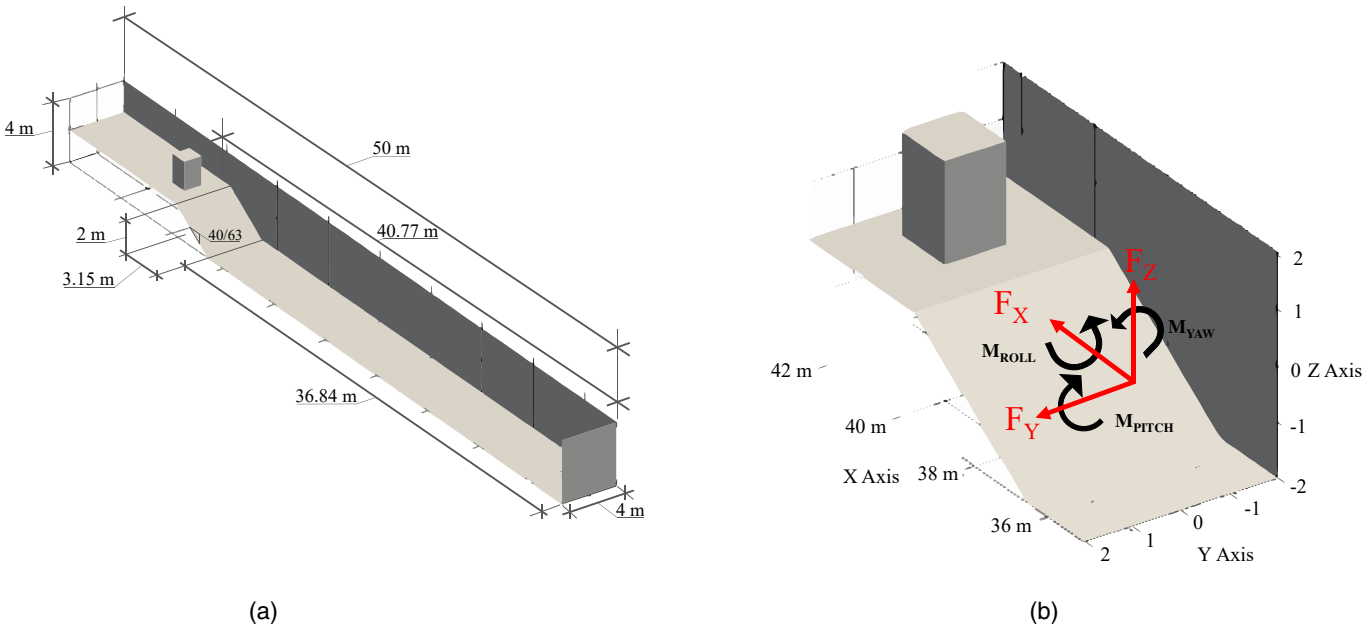

Fig. 10. Model dimensions: (a) flume; and (b) beach.

Table 4. Model boundary conditions for all field variables

Field	Atmosphere	Walls	Wavemaker
U	pressureInletOutletVelocity	noSlip	movingWallVelocity
p_{rgh}	totalPressure	fixedFluxPressure	fixedFluxPressure
ν_t	calculated	nutkWallFunction	nutkWallFunction
k	inletOutlet	kqRWallFunction	kqRWallFunction
ω	inletOutlet	omegaWallFunction	omegaWallFunction
ϵ	inletOutlet	epsilonWallFuction	epsilonWallFuction
α	inletOutlet	zeroGradient	zeroGradient
pointDisplacement	fixedNormalSlip/fixedValue	fixedNormalSlip/fixedValue	wavemakerMovement

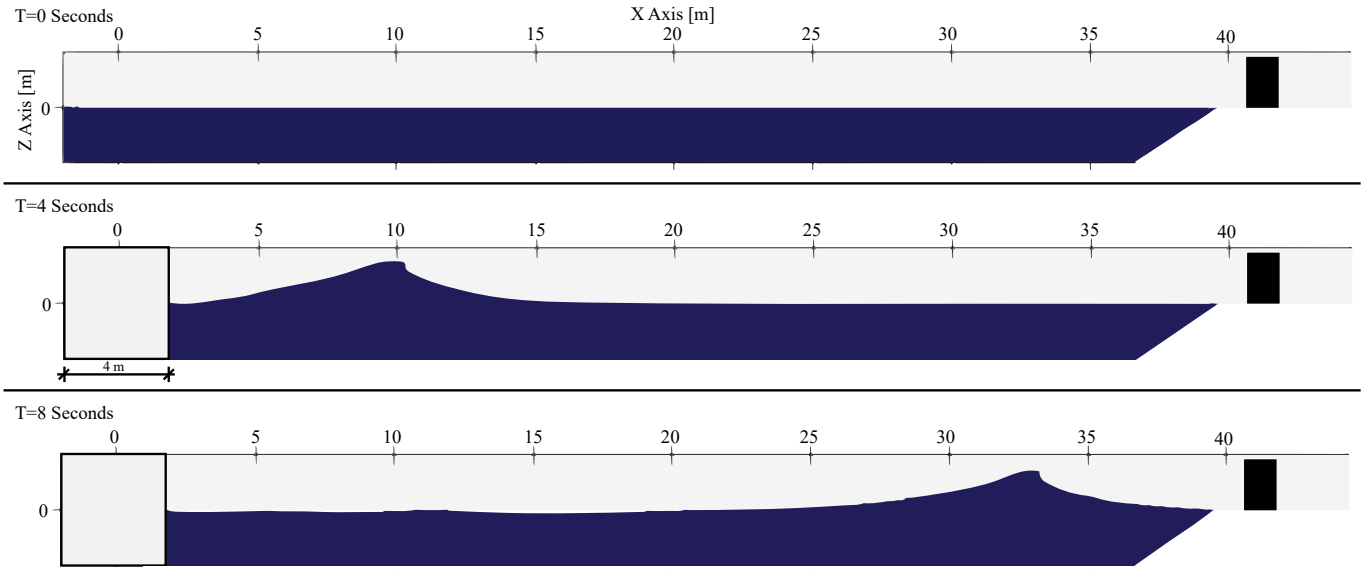

Fig. 11. Side elevation of OpenFOAM model at selected times.

travel down the flume as well as the end state (fully extended) of the prescribed motion of the wavemaker as the water moves toward the test specimen. Side-by-side comparisons of simulation results and videos obtained from experiment trials are shown in Figs. 12(a–c). General shapes of the free surface of the multiphase air–water mixture agreed well with those observed in videos of the experiments, with a reasonable resolution of the splashing of the fluid around the structure upon impact. As shown in Fig. 12(c), the experimental and numerical postimpact wake shapes behind the specimen matched well.

Experimental time histories of the free-surface height for the wave-gauge instruments and the calculated location of the free surface of the simulated fluid air–water boundary at identically located sample points within the computational model are shown for comparison in Fig. 13. The measured values for the free surface and the location of the free surface calculated in OpenFOAM show strong agreement. Velocities for ADVs 1 and 2 match well with velocities calculated in OpenFOAM. ADVs 3 and 4 experienced a large degree of noise from bubbles being created and collapsing, producing acoustic waves and the broken wave bore near the test structure. A comparison of ADV 3 with its associated OpenFOAM velocity probe are shown in Fig. 14; the figure shows the substantial amount of noise for ADV 3's measured values.

Table 5 shows that, with respect to the values for base shear and overturn moment calculated from the strain gauges upon the supporting CFTs and the forces obtained from the numerical model, shear and vertical forces were overmeasured by the load cells but overturn moments were undermeasured. This was assumed to be due to the presence of large magnitudes of water near the upstream face of the specimen weighing down the panels surrounding the specimen and, consequently, imparting the force of its weight on the load cells nearest the front of the structure and reducing their contribution to the overturn moment. This floor-loading phenomenon was simulated within OpenFOAM and compared to the measured values from the load cells, shown in the solid and dashed black lines of Fig. 15. Forces from the simulations upon the test specimen varied slightly from those obtained from the experiments, but the simulated force trends and magnitudes fell within 10 percent of the measured loads, which were unaffected by slight asymmetries in the test frame's stiffness. These differences need to be investigated in future research; however, the agreement between forces obtained from experiments and numerical models was assumed to be within an acceptable range for justifying further refinements to the modeling methodologies and advancement of the techniques implemented for tsunami resilience engineering purposes.

Contour plots of the pressure over the upstream face of the specimen obtained from OpenFOAM simulations and experiments at the instant the peak base shear occurred are shown in Fig. 16. The experimentally obtained pressures are shown in the right-hand panel—this contour was constructed by reflecting pressure measurements from all pressure sensors about the centerline of the specimen and using a cubic interpolation function between values of pressure at discrete locations. The signal from the pressure sensors utilized in the experiments seems to have been attenuated around the peak

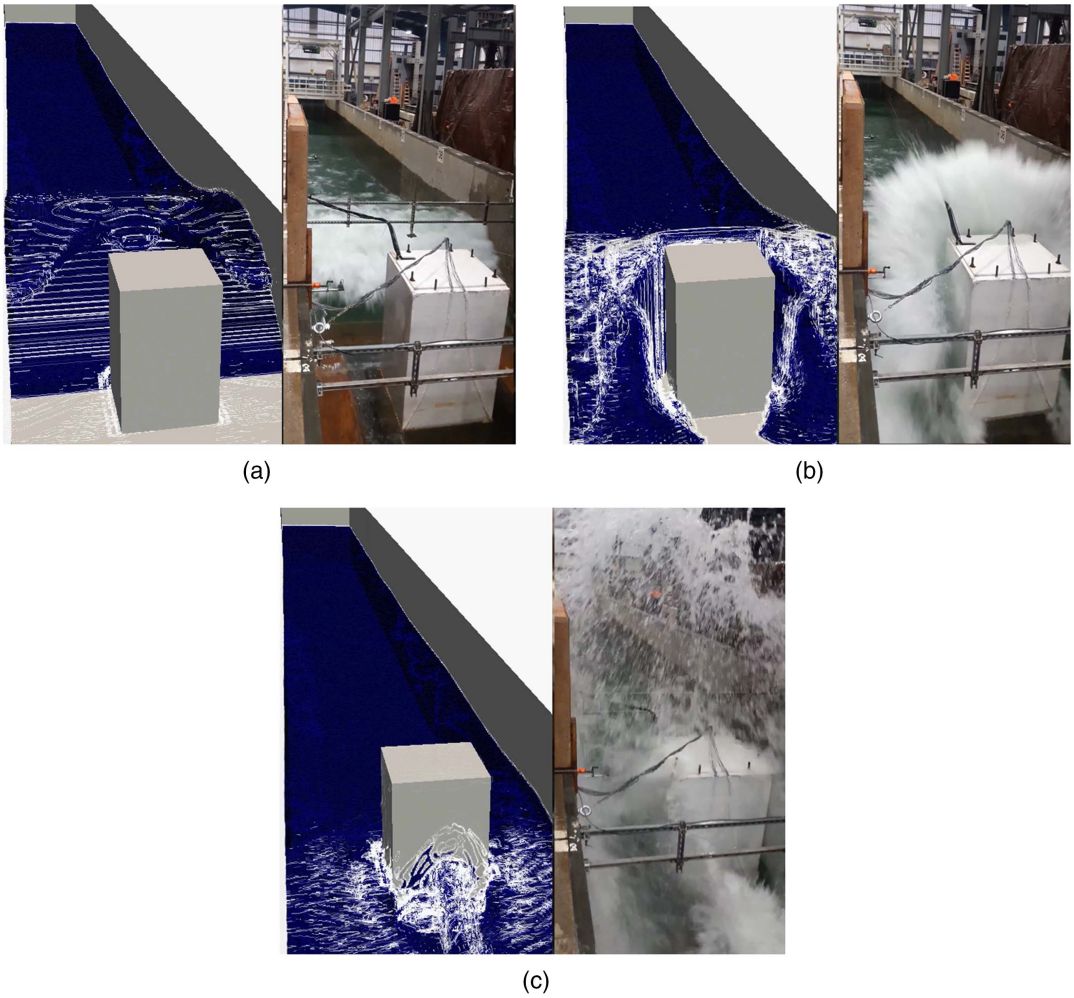

Fig. 12. Wave impact comparison: (a) preimpact; (b) impact; and (c) postimpact.

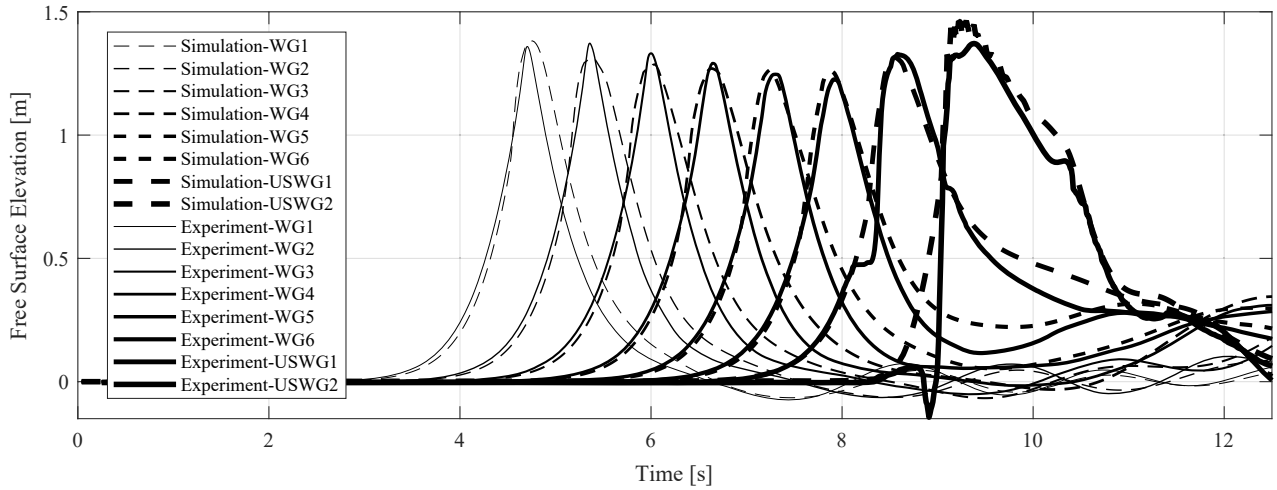

Fig. 13. Test simulation free surface height comparison: 1.45 m wave.

pressure; this was manifested as lower overall pressure magnitudes over the upstream face of the specimen at the instant of peak streamwise force. Consequently, the contours of the experimental and simulated pressures do not appear to match very well at the peak force instance; however, local pressure sensor location comparisons show reasonable agreement, with slight temporal and magnitude variations.

Pressure contours upon the upstream face of the specimen help determine the nature of the instantaneous and sustained loading profiles upon structural elements and walls subject to bore impact

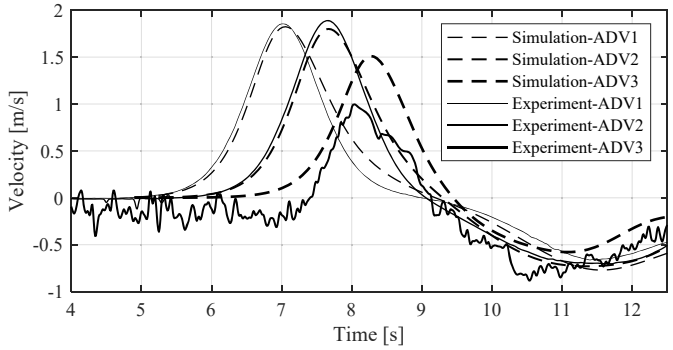

Fig. 14. Test simulation velocity comparison: 1.45 m wave.

Table 5. Wave force comparison for 1.45-m wave: simulated versus experimentally measured

Measurement origin	Fx (kN)	Fy (kN)	Fz (kN)	Mx (kN-m)	My (kN-m)	Mz (kN-m)
Strain gauges	25.74	0	11.13	2.28	24.31	0.41
Load cell	37.62	0.61	−106.09	0.8	22.41	2.57
Pressure sensors	25.91	0	0	0	0	0
Simulation	31.79	0	−111.01	0	22.65	0

and flow entrainment; the shape of the loading profile is significant in evaluating the force response of critical structural elements. Locally measured and simulated pressures showed strong agreement over the duration of the loading. This also applied to time-integrated pressure values and resultant impulses, particularly near the base of the structure, where cell sizes were smaller than higher up on the wall. Trial averaged pressure and impulse time histories at two representative points along the seaward face of the structure chosen for comparison of experimentally measured values and those simulated by the numerical model are shown in Figs. 17(a–d). These sensors, B06 and D11, were located near the center and near the lower right-hand corner of the specimen's upstream face, respectively. While pressures matched well at an order of magnitude, at the local level the pressure distribution over the face of the specimen could be better resolved temporally and spatially with a finer mesh in the plane perpendicular to the flow of the wave. It is presumed that due to the size of the cells, some averaging occurred between peaks and troughs in pressures that otherwise would have resulted in a closer match to experimental pressure measurements. For the current study the mesh was kept at a moderate level of refinement to keep numerical model run times within reasonable limits; this was deemed acceptable for the phenomenological purposes of this investigation.

Discussion

Evaluation of ASCE 7-16 Section 6.10.1 at Test Scale

The measured forces were compared with design equation forces using ASCE 7-16 and the experimental values for flow depth and velocity. Eqs. (1) and (2) were used to determine the estimated unbalanced hydrostatic loading described in Section 6.10.1 of ASCE 7-16

$$p_{uw} = 1.25 \times I_{\mathrm{TSU}} \times H_{\mathrm{MAX}} \times \gamma_s \tag{1}$$

where p_{uw} = pressure on the streamwise face of the structure due to a tsunami; I_{TSU} = importance factor for tsunami loading (from ASCE 7-16 Tables 6.8-1); H_{MAX} = minimum inundation depth at the site = 1.39 m; γ_s = density of seawater = 10.78 kN/m^3 × ks; and $ks = 1.1$ to account for suspended solids and other small debris in the tsunami flow

$$P_{\mathrm{TSU}} = 1.3 \times p_{uw} \times H_{\mathrm{MAX}} \times b_w \tag{2}$$

where P_{TSU} = streamwise force from tsunami inundation; p_{uw} = pressure from the tsunami, calculated by 1; H_{MAX} = minimum inundation depth at the site = 1.39 m; and b_w = width of the face of the building closest to the incoming wave = 1.17 m.

For this comparison, the experimental wave height was obtained from the closest wave gauge to the structure with statistically repeatable measurements, USWG2. For both the unbroken solitary wave and the spilling breaker, this was measured to be 1.39 m, and this value was used to calculate the total theoretical pressure and force on the structure without the 1.25 multiplier in Eq. (1) and the 1.3 multiplier in Eq. (2) and $I_{\mathrm{TSU}} = 1$ (rather than 1.25). Experimental forces were calculated from the pressure distribution over the face of the structure averaged over all trials per wave type. The results are shown in Table 6. The point of this exercise was to demonstrate that (through testing the core wall specimen subject to inundation at reduced scale then scaling up the forces obtained from experimentation by Froude number similitude) forces measured and extrapolated compared well to the ASCE 7-16 demands calculated without safety factors or importance factors. The results show

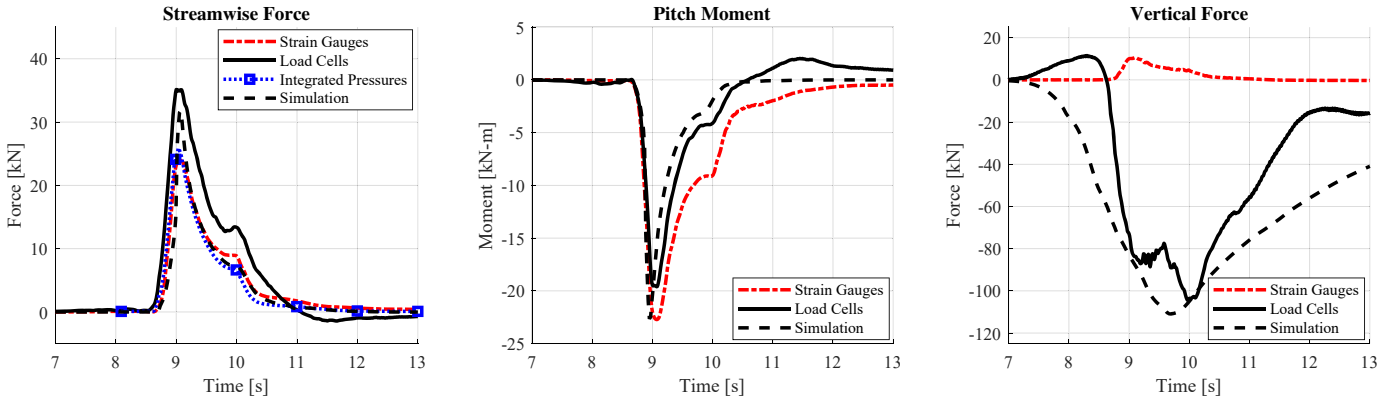

Fig. 15. Wave impact forces—comparison between trial averaged experimental and simulated principal forces and overturn moment. Experimental streamwise forces were measured through load cells, pressure sensors, and strain gauges. Simulated forces were calculated with OpenFOAM.

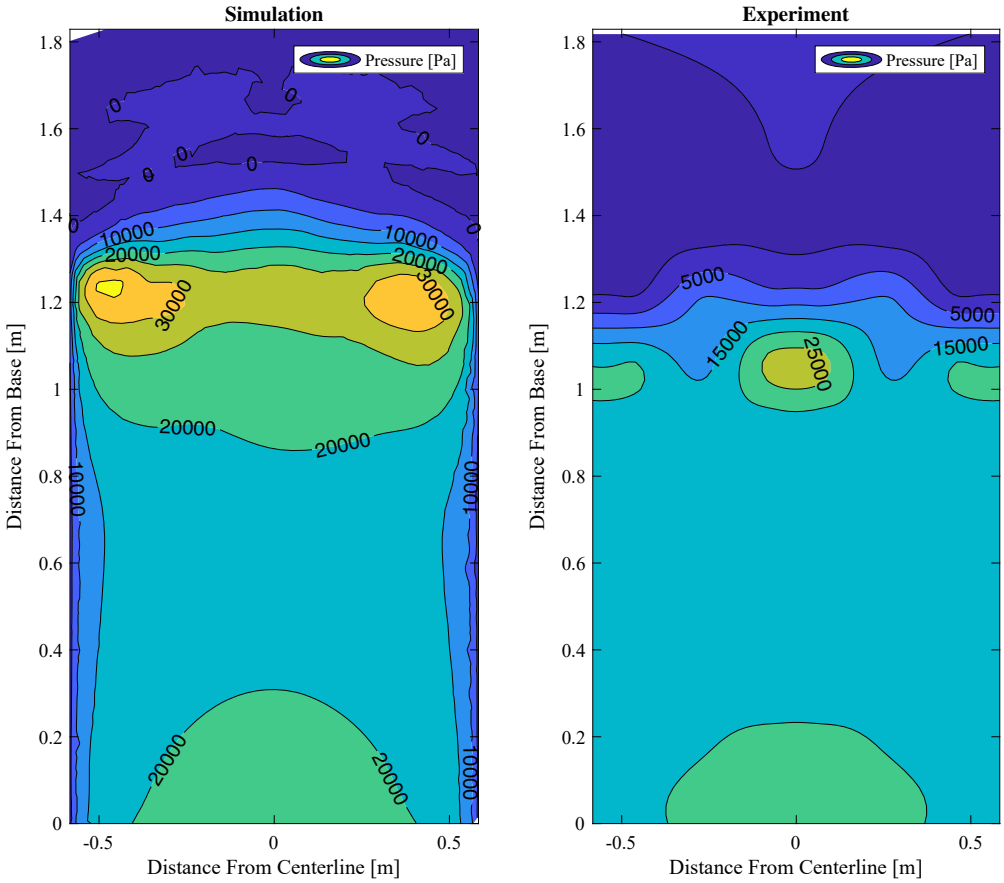

Fig. 16. Trial averaged upstream face pressures at peak base shear (time = 9 s).

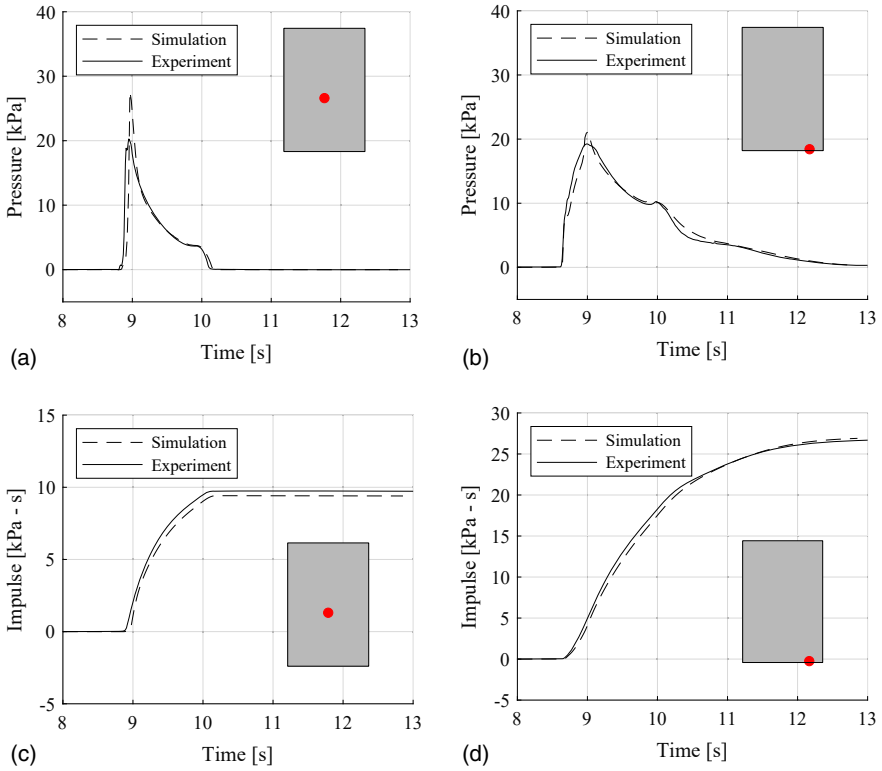

Fig. 17. Trial averaged pressure and time-integrated pressure time histories for two representative seaward face sensors, B06 and D11: (a) B06 pressure; (b) D11 pressure; (c) B06 time-integrated pressure; and (d) D11 time-integrated pressure.

Table 6. ASCE 7-16 equation 6.10–1: comparison to experimental results

Wave height (m)	H_{MAX} (m)	I_{TSU}	$\gamma_s\left(\frac{kN}{m^3}\right)$	$p_{uw}\left(\frac{kN}{m^2}\right)$	B_w (m)	P_{TSU} (kN)	P_{EXP} (kN)	Error (%)
1.40	1.39	1	10.78	15.03	1.17	24.47	23.46	4.31
1.45	1.39	1	10.78	15.03	1.17	24.46	25.91	5.90

Table 7. ASCE 7-16 Section 6.6 site topology transect results scaled to 1:6 by means of hydrodynamic similitude using Froude number scaling (length scale $\lambda = 6$, velocity scale $\lambda^{0.5} = \sqrt{6}$)

Fluid height source	EGL	1:6 EGL	Experiment
Inundation depth (m)	7.99	1.33	1.39
Flow velocity $\left(\frac{m}{s}\right)$	8.90	3.63	5.82 (celerity)

that the expressions estimated the force well, with a maximum difference between the theoretical force and the measured force of under six percent. It is important to note that despite this comparison matching very well, the fluid elevation was the only variable of concern in this equation. In addition, fluid elevation was not measured directly at the specimen, but at USWG2, 0.8 m upstream from the front face of the specimen—differences in fluid elevation between this location and the upstream face of the specimen could lead to variations in prediction accuracy.

Extrapolation of Demands from Experiments to Full Structural Scale Representative Vertical Evacuation Structure

The measured forces imparted to the specimen scaled to representative VES dimensions by the means of Froude number similitude (length scale factor of $\lambda = 6$, force scale factor of $\lambda^3 = 216$, work and moment scale factor of $\lambda^4 = 1{,}296$) indicated that a structure geometrically similar to the one tested at realistic building scales would experience 5.56 MN ($\lambda^3 \times 25.74$ kN) of base shear from the initial bore impact in combination with an overturn moment of 31.0 MN·m ($\lambda^4 \times 24.31$ kN·m). Initial ASCE 7-16 calculations for prediction of design forces offered 65.7 MN as the total base shear to the full seaward face of the structure (45.72 m wide). Reduction of this force by the ratio of the width of the shear wall in cross flow to the ratio of the full width of the structure (7.01:45.72 m = 1:6.52) gives 10.08 MN as the force predicted by ASCE 7-16's equation for inundation force imparted to the core wall due to an inundation at the height predicted by the energy grade line (EGL) method and corresponding sections of the design provisions. Reduction of this calculated value by the amplification factors applied to pressure and density values within Eqs. (1) and (2) ($1.3 \times 1.1 \times 1.25 = 1.7875$) yielded 5.63 MN, which was within 1.5% of the experimentally measured force.

It is important to note that the waves considered in this study were not truly representative of those that would be experienced in a tsunami, and no effort was made during experimentation to match the wave height and speed at similitude within the flume to the inundation heights and velocities calculated by the EGL method from the preliminary design of the representative VES. It is also important to note that due to the difficulty in scaling experiments that are hydrodynamically similar to tsunamis to realistic building scales, not many testing facilities currently offer small-scale (geometric scale within 1:6 to 1:10) testing procedures that will scale appropriately to tsunami wave lengths. Consequently, the paddle-driven wave methodologies presented here were considered the best available science to the researchers. With a fluid elevation in the experiments close to that of the EGL method at 1:6 scale (Table 7), the forces from the presented experiments scale following Froude number similitude laws closely ($\text{Force}_{\text{LargeScale}} = \lambda^3 \times \text{Force}_{\text{SmallScale}}$) to tsunami hydrostatic inundation forces predicted via the EGL method (Table 8).

Table 8. Force results: comparison of ASCE 7-16 Section 6.6 site topology transect calculated inundation base shear force with experimentally scaled shear force using Froude number hydrodynamic similitude (length scale $\lambda = 6$, force scale $\lambda^3 = 216$)

Base shear source	EGL	EGL (no amplifiers)	$\lambda^3\times$ experiment
Maximum force (MN)	10.08	5.63	5.56

Conclusions

In summary, preliminary numerical models were utilized to determine specimen and instrument placement as well as the flume bathymetry to be used in experimentation. Experiments were then conducted, and simulations of the experiments were created from the information obtained from these experiments. The results from the simulations were then correlated with experimentally measured values for specimen reaction force, fluid velocity, fluid elevation, and local dynamic pressure at several locations, and measured demands were compared to theoretical expected values for demand according to measured variables.

Changing the soil level had little effect on load transfer to the soil box base slab. The total shear in the piles showed only a slight increase from the full to the empty soil box condition. Total shear also showed a decrease in force between the full and half-full soil box experiments. More strain gauges need to be used to understand axial force in piles. The total axial force on the specimen as measured by the strain gauges varied between the top and bottom strain gauge locations, indicating that something was off with their measurements. This may have been due to the angles for attaching the moving braces welded to the piles about 3.8 cm above the top strain gauges. Due to the close proximity of the strain gauges to this discontinuity in the section axial strains may have not redistributed evenly by the time they reached the top strain gauges, invalidating the assumption that strains varied linearly between the strain gauges on the front and back of the piles. Additional strain gauges placed in the middle of the piles would help to better understand the distribution of strains in the piles.

A spilling breaker wave induces a greater streamwise force on a test specimen than an unbroken solitary wave of roughly the same height. All three methods of measuring streamwise force showed a 10%–15% increase in force between the unbroken solitary wave and the spilling breaker wave. Similar centerline pressure distributions and pressure distribution centroid locations were found for both wave types. The pressures recorded for the 1.45-m wave were slightly higher, however, and showed a sharper decrease in pressures near the top of the wall.

It was found that Eqs. (1) and (2) taken from Section 6.10.1 of ASCE 7-16 did a good job of estimating the total force from the tsunami waves on the test specimen when the safety factors were removed from the equation. ASCE 7-16 offers a simplistic, yet conservative approach for reasonable approximation of tsunami wave

inundation force. This demonstrates that the provided equations are valid for a wide range of scenarios. It also implies that work can be done to improve the equations so that they are more applicable to a specific set of scenarios; this would be beneficial for tsunami-resilient design. Though overall magnitudes of force may be estimated properly, the possibility of these loads fluctuating is not something that was accounted for. Assumptions can be made about the nature and shape of the loading profile from the tsunami inundation, but without a comprehensive analysis of the fluid behavior in and around the structure, the true nature of the interaction between the tsunami and the structure cannot be known. Without a thorough understanding of the load flow of the tsunami wave inundation through the structure to the ground, from the structure to the foundation, and from the foundation to the surrounding soil, we may not truly understand the demands on structures subject to such events.

While the equations provided by the standard did a good job of estimating the overall magnitude of force for a given inundation height, our tests using paddle driven waves showed that there are parameters such as bore type and local fluid velocity that may have a considerable effect on the forces imparted against structures. Local fluid effects due to these parameters cannot be predicted for all wave types by the equations; therefore, it may be of interest to investigate higher fidelity modeling methods that can offer better opportunities for understanding how we can improve resilience. The OpenFOAM simulation did a good job of predicting the free surface elevation and velocity of the wave tested experimentally, with free surface elevation and velocities showing differences between simulation and experiment of less than 4% on average. The computed simulation pressures varied more from the experimental pressures, with large differences observed between the experimental pressure distribution and the simulated pressure distribution. While the experiments seemed to show a linear decrease up the height of the wall, the simulations showed lower pressures at the bottom of the wall and larger pressures in the middle of the wall. Total force from the experiment was overestimated in the OpenFOAM simulation by about 10%.

Because more complicated testing methodologies involving wave generation methods that would most resemble tsunamis at full scale are rare and expensive, it may be of use to investigate numerical methods such as CFD for determination of appropriate demands to structures at full scale, because cost, time schedule, and feasibility are far less of a hurdle in numerical simulations at full scale than in experimentation at full scale. By validating numerical models of experiments conducted at a reduced scale, validated models can be used to simulate events at full scale in order to assess the accuracy of design equations. In order to determine actual forces and impulses imparted against structures from tsunami inundation events, it may be necessary to expand the numerical analysis size to realistic length scales for design of structures subject to tsunamis. Therefore, the intention in future research is to expand the modeling methodology so that the validated simulation methodologies can be utilized for the purposes of simulation of full-scale structural responses to extreme hydrodynamic impulses. The validated methodologies will assist engineers in determining tsunami forces at realistic scales when testing prototypical structures is not feasible or when experimental results from small-scale tests cannot be extrapolated accurately beyond their test scales.

Data Availability Statement

Some or all data, models, or code that support the findings of this study are available from the corresponding author upon reasonable request.

Acknowledgments

The authors thank the National Science Foundation and Joy Pauschke (program manager) for their financial support of this project through Grant Nos. CMMI-1726326 and CMMI-1933184. This work was facilitated through the use of advanced computational, storage, and networking infrastructure provided by the Hyak supercomputer system, supported in part by the University of Washington eScience Institute. Experimental work was conducted by a collaborative team from the University of Washington and Oregon State University led by Master's Students Christopher Pyke and Kenneth Sullivan. Simulations and computational analysis were completed by Nicolette Lewis from the University of Washington with the assistance of Andrew O. Winter, Ph.D., Dawn E. Lehman, Ph.D., Michael R. Motley, Ph.D., Pedro Arduino, Ph.D., and Charles W. Roeder, Ph.D. The authors and advisory committee would like to thank the faculty and staff at Hinsdale Wave Research Laboratory for their contributions to this project and all others who assisted with experimentation and data curation.

References

ASCE. 2017. *Minimum design loads and associated criteria for buildings and other structures*. ASCE 7-16. Reston, VA: ASCE.

Atwater, B. F., S. Musumi-Rokkaku, K. Satake, Y. Tsuji, K. Ueda, and D. K. Yamaguchi. 2015. *The orphan tsunami of 1700—Japanese clues to a parent earthquake in North America*. 2nd ed., 135. Seattle: University of Washington Press.

Baiguera, M., T. Rossetto, I. Robertson, and C. Petrone. 2019. *A nonlinear static procedure for the tsunami design of a reinforced concrete building*. Reston, VA: ASCE.

Baiguera, M., T. Rossetto, I. N. Robertson, and C. Petrone. 2022. "A procedure for performing nonlinear pushover analysis for tsunami loading to ASCE 7." *J. Struct. Eng.* 148 (2): 04021270. https://doi.org/10.1061/(ASCE)ST.1943-541X.0003256.

Chock, G., L. Carden, I. Robertson, M. Olsen, and G. Yu. 2013. "Tohoku tsunami-induced building failure analysis with implications for USA tsunami and seismic design codes." *Earthquake Spectra* 135 (1): 021601. https://doi.org/10.1193/1.4000113.

Chock, G., G. Yu, H. K. Thio, and P. J. Lynett. 2016. "Target structural reliability analysis for tsunami hydrodynamic loads of the ASCE 7 standard." *J. Struct. Eng.* 142 (11): 04016092. https://doi.org/10.1061/(ASCE)ST.1943-541X.0001499.

Chock, G. Y. K. 2016. "Design for tsunami loads and effects in the ASCE 7-16 standard." *J. Struct. Eng.* 142 (11): 04016093. https://doi.org/10.1061/(ASCE)ST.1943-541X.0001565.

Chock, G. Y. K., L. Carden, I. Robertson, Y. Wei, R. Wilson, and J. Hooper. 2018. "Tsunami-resilient building design considerations for coastal communities of Washington, Oregon, and California." *J. Struct. Eng.* 144 (8): 04018116. https://doi.org/10.1061/(ASCE)ST.1943-541X.0002068.

Foster, A., T. Rossetto, and W. Allsop. 2017. "An experimentally validated approach for evaluating tsunami inundation forces on rectangular buildings." *Coastal Eng.* 128 (5): 44–57. https://doi.org/10.1016/j.coastaleng.2017.07.006.

Gills, C. J. 2018. "Experimental and numerical validation of three-dimensional tsunami wave pressures and forces on an elevated structure." M.S. thesis, Univ. of Washington.

Heintz, J., and M. Mahoney. 2008. "Guidelines for design of structures for vertical evacuation from tsunamis." In *Proc., 14th World Conf. on Earthquake Engineering*. Tokyo: International Association for Earthquake Engineering.

Higuera, P. 2018. "Phicau/olaFlow: CFD for waves (v1.1)." Accessed June 24, 2018. https://zenodo.org/record/1297013#.YyRCHHZBzcd.

Hirt, C. W., and B. D. Nichols. 1981. "Volume of fluid (VOF) method for the dynamics of free boundaries." *J. Comput. Phys.* 39: 201–225. https://doi.org/10.1016/0021-9991(81)90145-5.

Lynett, P. J. 2009. "Tsunami inundation, modeling of." In *Complexity in tsunamis, volcanoes, and their hazards*, 117–133. Berlin: Springer. https://doi.org/10.1007/978-1-0716-1705-2_569.

Madsen, P. A., D. R. Fuhrman, and H. A. Schäffer. 2008. "On the solitary wave paradigm for tsunamis." *J. Geophys. Res. Oceans* 113 (12): 4932. https://doi.org/10.1029/2008JC004932.

Melton, J. E., D. D. Robertson, and S. A. Moyer. 1989. *An integrated CFD/experimental analysis of aerodynamic forces and moments*. Moffett Field, CA: National Aeronautics and Space Administration.

Menter, F. R., M. Kuntz, and R. Langtry. 2003. "Ten years of industrial experience with the SST turbulence model." In *Proc., 8th Annual Int. Bridge Conf., Int. Symp. on Turbulence, Heat and Mass Transfer*, 625–632. Antalya, Turkey: Begell House.

Motley, M. R., H. K. Wong, X. Qin, A. O. Winter, and M. O. Eberhard. 2016. "Tsunami-induced forces on skewed bridges." *J. Waterw. Port Coastal Ocean Eng.* 142 (3): 04015025. https://doi.org/10.1061/(ASCE)WW.1943-5460.0000328.

Petersen, M. D., et al. 2014. *Documentation for the 2014 update of the United States national seismic hazard maps*. US Geological Survey Open-File Rep. 2014–1091. Reston, VA: USGS.

Pyke, C. N. 2020. "Testing of a reinforced concrete core wall for tsunami vertical evacuation shelter structures in a wave flume." M.S. thesis, Dept. of Civil and Environmental Engineering, Univ. of Washington.

Qin, X., M. Motley, R. Leveque, F. Gonzalez, and K. Mueller. 2018. "A comparison of a two-dimensional depth averaged flow model and a three-dimensional rans model for predicting tsunami inundation and fluid forces." *Nat. Hazards Earth Syst. Sci.* 18 (Jan): 56.

Robertson, I., and A. Mohamed. 2009. "Development of performance based tsunami engineering, PBTE." In *Proc., IABSE Symp. Report*, 16–23. Alexandria, VA: National Science Foundation.

Rossetto, T., C. De la Barra, C. Petrone, J. C. De la Llera, and J. Vásquez, and M. Baiguera. 2019. "Comparative assessment of nonlinear static and dynamic methods for analysing building response under sequential earthquake and tsunami." *Earthquake Eng. Struct. Dyn.* 48: 867–887. https://doi.org/10.1002/eqe.3167.

Rossetto, T., C. Petrone, I. Eames, C. De La Barra, A. Foster, and J. Macabuag. 2018. "Advances in the assessment of buildings subjected to earthquakes and tsunami." In Vol. 46 of *Proc., European Conf. on Earthquake Engineering: Recent Advances in Earthquake Engineering in Europe*, edited by K. Pitilakis, 545–562. Cham, Switzerland: Springer. https://doi.org/10.1007/978-3-319-75741-4_23.

Rueben, M., R. Holman, D. Cox, S. Shin, J. Killian, and J. Stanley. 2011. "Optical measurements of tsunami inundation through an urban waterfront modeled in a large-scale laboratory basin." *Coastal Eng.* 58 (5): 229–238. https://doi.org/10.1016/j.coastaleng.2010.10.005.

Seiffert, B. R., R. C. Ertekin, and I. N. Robertson. 2015. "Wave loads on a coastal bridge deck and the role of entrapped air." *Appl. Ocean Res.* 53 (Jul): 91–106. https://doi.org/10.1016/j.apor.2015.07.010.

Shafiei, S., B. W. Melville, and A. Y. Shamseldin. 2016. "Experimental investigation of tsunami bore impact force and pressure on a square prism." *Coastal Eng.* 110 (5): 1–16. https://doi.org/10.1016/j.coastaleng.2015.12.006.

Swigler, D. T. 2009. "Laboratory study investigating the three-dimensional turbulence and kinematic properties associated with a breaking solitary wave." Master's thesis, Texas A&M Univ. https://hdl.handle.net/1969.1/ETD-TAMU-2009-08-821.

Weller, H. G. 1998. "Openfoam: A tensorial approach to computational continuum mechanics using object-oriented techniques." *Comput. Phys.* 12 (6): 168744. https://doi.org/10.1063/1.168744.

Wienke, J., and H. Oumeraci. 2005. "Breaking wave impact force on a vertical and inclined slender pile—Theoretical and large-scale model investigations." *Coastal Eng.* 52 (Dec): 435–462. https://doi.org/10.1016/j.coastaleng.2004.12.008.

Wilson, J., R. Gupta, J. Lindt, M. Clauson, and R. Garcia. 2009. "Behavior of a one-sixth scale wood-framed residential structure under wave loading." *J. Perform. Constr. Facil.* 23 (8): 9. https://doi.org/10.1061/(ASCE)CF.1943-5509.0000039.

Winter, A. O. 2019. "Effects of flow shielding and channeling on tsunami-induced loading of coastal structures." Ph.D. thesis, Dept. of Civil and Environmental Engineering, Univ. of Washington.

Winter, A. O., M. S. Alam, K. Shekhar, M. R. Motley, M. O. Eberhard, A. R. Barbosa, P. Lomonaco, P. Arduino, and D. T. Cox. 2020. "Tsunami-like wave forces on an elevated coastal structure: Effects of flow shielding and channeling." *J. Waterw. Port Coastal Ocean Eng.* 146 (4): 04020021. https://doi.org/10.1061/(ASCE)WW.1943-5460.0000581.

Xiang, T., D. Istrati, S. C. Yim, I. G. Buckle, and P. Lomonaco. 2020. "Tsunami loads on a representative coastal bridge deck: Experimental study and validation of design equations." *J. Waterw. Port Coastal Ocean Eng.* 146 (5): 04020022. https://doi.org/10.1061/(ASCE)WW.1943-5460.0000560.

Yang, Z., B. Huang, B. Zhu, J. Zhang, and A. Kang. 2021. "Comparative study of tsunami-like wave-induced forces on medium-scale models of box girder and t-girder bridges." *J. Bridge Eng.* 26 (2): 04020125. https://doi.org/10.1061/(ASCE)BE.1943-5592.0001671.